Title

Cell-cycle fate-monitoring distinguishes individual chemosensitive and chemoresistant cancer cells in drug-treated heterogeneous populations demonstrated by real-time FUCCI imaging

Journal

Cell Cycle, 14(4)

ISSN

1538-4101

Authors

Miwa, Shinji
Yano, Shuya
Kimura, Hiroaki
et al.

Publication Date

2015-02-16

DOI

10.4161/15384101.2014.991604

Peer reviewed

Cell Cycle 14:4, 621–629; February 15, 2015; © 2015 Taylor & Francis Group, LLC

Cell-cycle fate-monitoring distinguishes individual chemosensitive and chemoresistant cancer cells in drug-treated heterogeneous populations demonstrated by real-time FUCCI imaging

Shinji Miwa[1,2,3,†], Shuya Yano[1,2,4,†], Hiroaki Kimura[3], Mako Yamamoto[1,2], Makoto Toneri[1,2], Yasunori Matsumoto[1,2], Fuminari Uehara[1,2], Yukihiko Hiroshima[1,2], Takashi Murakami[1,2], Katsuhiro Hayashi[3], Norio Yamamoto[3], Michael Bouvet[2], Toshiyoshi Fujiwara[4], Hiroyuki Tsuchiya[3], and Robert M Hoffman[1,2,*]

[1]AntiCancer; Inc.; San Diego, CA USA; [2]Department of Surgery; University of California; San Diego, CA USA; [3]Department of Orthopedic Surgery; Kanazawa University Graduate School of Medical Sciences; Kanazawa, Ishikawa, Japan; [4]Division of Surgical Oncology; Department of Surgery; Okayama University Graduate School of Medicine; Dentistry and Pharmaceutical Sciences; Okayama, Japan

[†]These authors contributed equally to this work.

Keywords: cancer, cell cycle, chemoresistance, chemosensitivity, cisplatinum, doxorubicin, FUCCI, GFP, RFP, HeLa, time-lapse imaging, tumor heterogeneity

Essentially every population of cancer cells within a tumor is heterogeneous, especially with regard to chemosensitivity and resistance. In the present study, we utilized the fluorescence ubiquitination-based cell cycle indicator (FUCCI) imaging system to investigate the correlation between cell-cycle behavior and apoptosis after treatment of cancer cells with chemotherapeutic drugs. HeLa cells expressing FUCCI were treated with doxorubicin (DOX) (5 μM) or cisplatinum (CDDP) (5 μM) for 3 h. Cell-cycle progression and apoptosis were monitored by time-lapse FUCCI imaging for 72 h. Time-lapse FUCCI imaging demonstrated that both DOX and CDDP could induce cell cycle arrest in S/G_2/M in almost all the cells, but a subpopulation of the cells could escape the block and undergo mitosis. The subpopulation which went through mitosis subsequently underwent apoptosis, while the cells arrested in S/G_2/M survived. The present results demonstrate that chemoresistant cells can be readily identified in a heterogeneous population of cancer cells by S/G_2/M arrest, which can serve in future studies as a visible target for novel agents that kill cell-cycle-arrested cells.

Introduction

Many years ago, Levan and Hauschka,[1] Klein and Klein,[2] Makino,[3] Henderson and Rous,[4] Gray and Pierce,[5] Prehn,[6] Mitelman,[7] Foulds,[8,9] Fidler and Kripke,[10] observed multiple cancer-cell subpopulations within a tumor or cancer cell line. Gitone and Fidler[11] observed that spontaneous mutation rates are greater in metastatic cancer than in nonmetastatic subpopulations. Somatic cell fusion, as well as mutation, give rise to variants in a population of cancer cells.[12-14]

Tumor heterogeneity can give rise to chemosensitive and chemoresistant subpopulations within a tumor whose interaction can result in unexpected responses. Shifts in the ratios within tumor subpopulations can be a barrier to therapy.[15]

Goldie and Goldman[16] showed that early and combination therapy is necessary to overcome tumor heterogeneity.[14]

A thymidylate synthetase inhibitor caused a significant level of DNA damage in 58% of the cancer cells treated, but 25% of the cells had little or no damage. Using an imageable cell colony forming assay (iCFA), 2.6% of the treated cells were shown to maintain a colony growth rate similar to that of control colonies. Such minority resistant populations could account for tumor recurrence.[17]

Slocum et al.[18] determined the level of chemosensitivity heterogeneity of individual cancer cells in a population by time-lapse video imaging of the fate of sister post-mitotic cancer cells after treatment with a thymidylate synthetase inhibitor.[19,20] Immediate loss of cell division occurred in 74% of treated cells, but 6% of the cells could divide more than 2 times. The more proliferative sister-cell sibling could produce up to 73 times more cells than the other sister in the treated population, a striking demonstration of heterogeneity in sister cells after mitosis.

*Correspondence to: Robert M Hoffman; Email: all@anticancer.com
Submitted: 10/31/2014; Revised: 11/18/2014; Accepted: 11/20/2014
http://dx.doi.org/10.4161/15384101.2014.991604

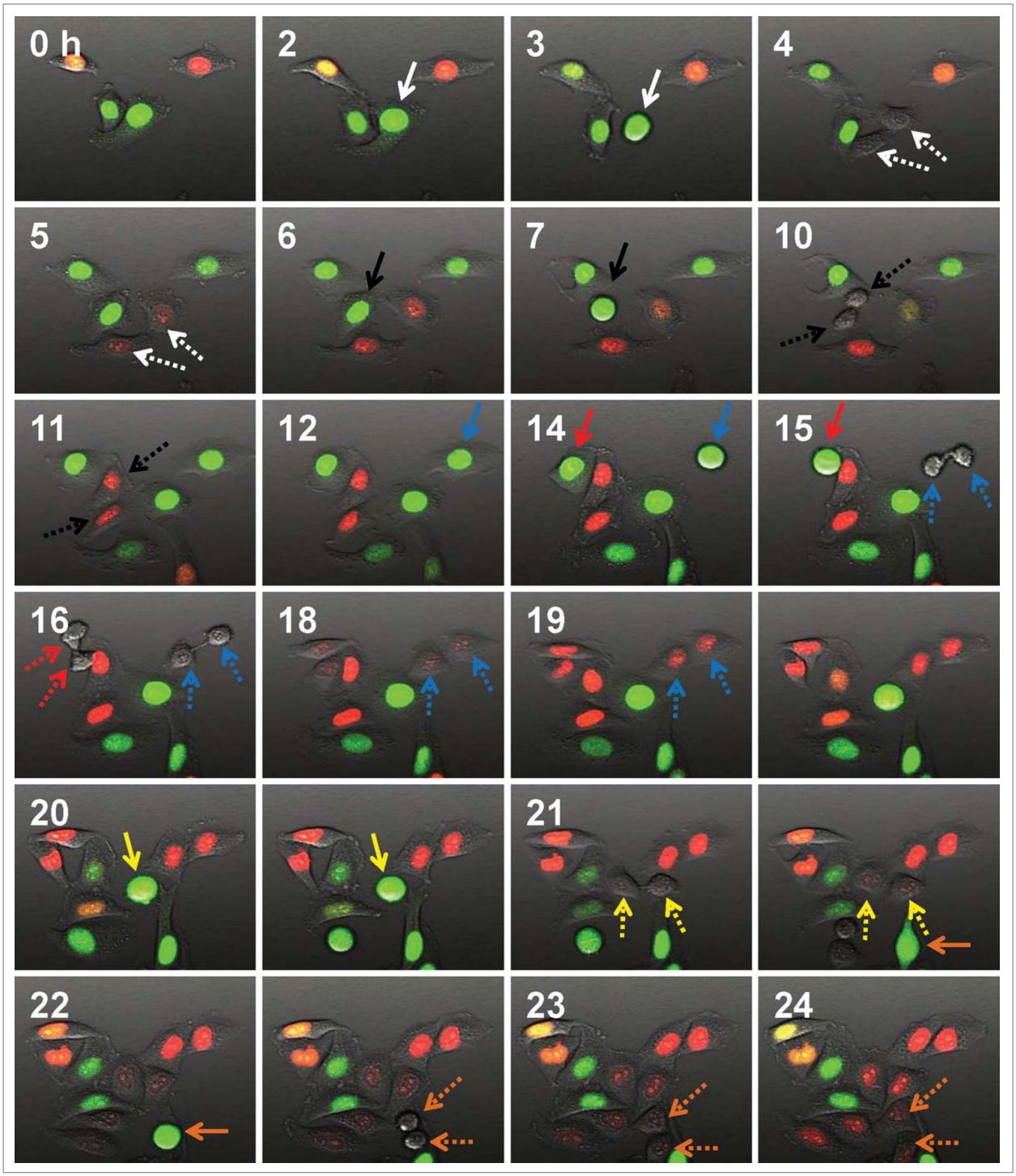

Figure 1. Time-lapse FUCCI imaging of cell-cycle progression in HeLa cells. The cells drew in their processes and became spherical before mitosis. Green fluorescence, indicating S/G_2 phase, became extinguished when the cells divided. Red fluorescence, indicating G_0/G_1 phase, gradually appeared in the newly-divided cells. The cells subsequently changed their fluorescence from red to yellow, followed by green indicating cell cycle progression. Solid and dotted arrows indicate the cells before and after mitosis, respectively.

The basis of tumor heterogeneity is still poorly understood. Both genetic and non-genetic mechanisms could account for phenotypic heterogeneity.[21]

Intermixed, juxtaposed populations of cells within a tumor have been shown to have distinct genotypes. For example, cancer cells with *MET* amplification, epidermal growth factor receptor (EGFR) amplification, and PDGFR [platelet-derived growth factor receptor 1] amplification have been shown in a single tumor. It has been suggested that tumor cell populations may subspecialize to support each other.[21]

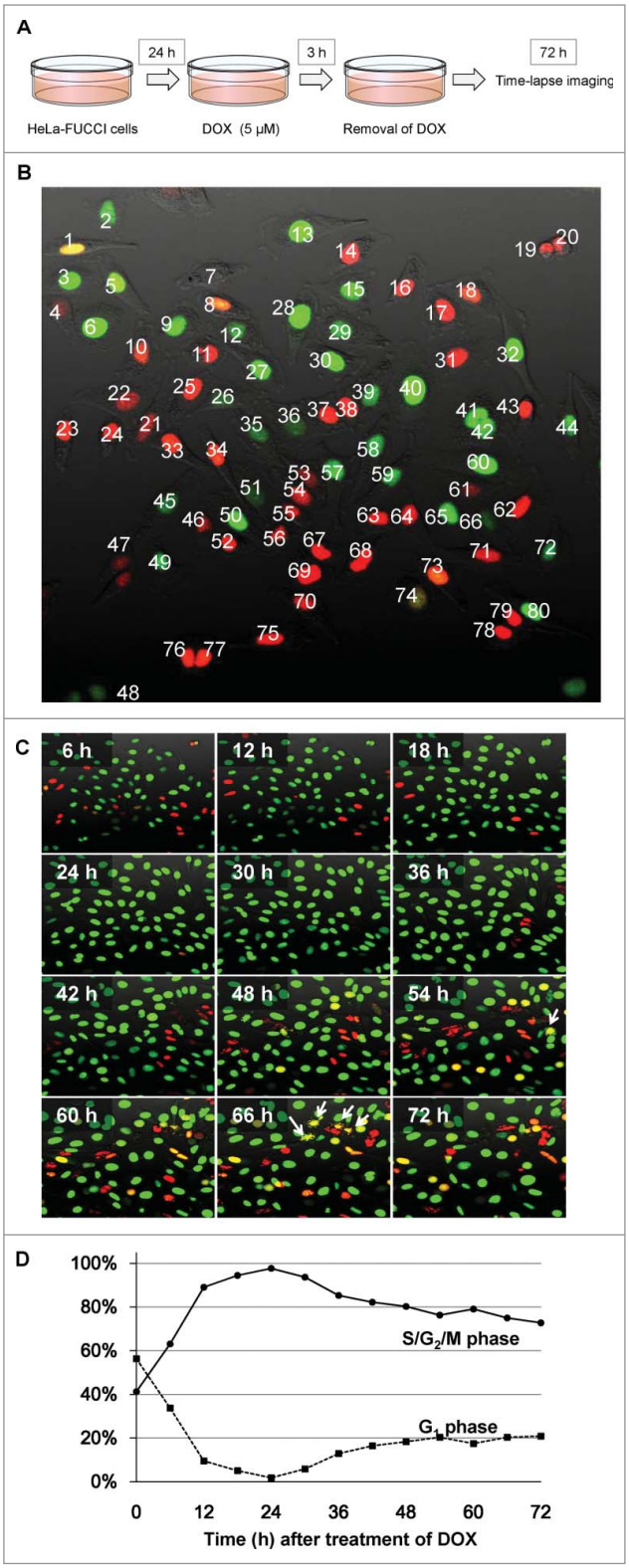

Figure 2. Single-cell time-lapse FUCCI imaging in HeLa cells after treatment with DOX. (**A**) Study protocol. (**B**) Each cell was individualized by numbering, and the cell cycle phase of each cell was observed for 72 hours. (**C**) Cell cycle modulation and apoptosis induced by DOX. Arrows indicate apoptotic cells. (**D**) Time-course distribution of cell-cycle phase after DOX treatment.

Table 1. Cell cycle fate analysis of HeLa-FUCCI cells after DOX treatment

Parameters	Cell No.
Cell cycle phase at the beginning of time-lapse imaging	
G_0/G_1 phase	118 (59.6%)
$S/G_2/M$ phase	80 (40.5%)
G_1/S transition during time-lapse imaging	
yes	88 (44.4%)
no	110 (55.6%)
Mitosis during time-lapse imaging	
yes	81 (40.9%)
no	117 (59.1%)
Cell cycle "reversal" during time-lapse imaging	
Yes	9 (4.5%)
No	189 (95.4%)
Apoptosis during time-lapse imaging	
Yes	97 (49.0%)
No	101 (51.0%)

Cells changing fluorescence color from FUCCI green to red without entering mitosis.

Sakaue-Sawano et al.[22] have utilized oscillating proteins linked to spectrally-distinct fluorescent proteins that specifically mark cell cycle phases in order to image cell cycle kinetics, in a system termed FUCCI (fluorescence ubiquitination-based cell cycle indicator). Using the FUCCI system, which reports what phase of the cell cycle a cell may reside, with quiescent cells expressing a red fluorescent protein (RFP) and cycling cells expressing a green fluorescent protein (GFP), we observed at the surface of a tumor, approximately 80% of the cells are green or yellow-green indicating they are cycling, but deeper within the tumor, approximately 90% of the cells are resting and remain so. Chemotherapy killed only the surface cells of the tumor with the remaining cells remaining quiescent and thereby resistant. After chemotherapy, a new set of proliferating surface cells appeared.[23] Overcoming cell-cycle arrest, observed by FUCCI imaging, has been shown to enhance efficacy of anticancer drugs.[24,25]

There are a number of reports about the phase of cell cycle arrest induced by anticancer agents.[26-28] The present study correlates cell cycle arrest and survival after chemotherapy at the single-cell level, in real-time, using FUCCI imaging of a heterogeneous cancer-cell population. This new means of observing heterogeneity of response to chemotherapy of individual cancer cells can provide novel visual targets to eradicate such resistant cells.

Results and Discussion

Time-lapse imaging of cell-cycle progression in HeLa-FUCCI cells

Time-lapse fluorescence imaging of HeLa-FUCCI cells was performed every 30 min for 72 h (**Fig. 1**, Supp. Video 1). FUCCI green-fluorescent cycling cells drew in their processes and had a spherical shape during mitosis (**Fig. 1**). After mitosis, red fluorescence appeared in the cells after division, indicating entry to G_0G_1

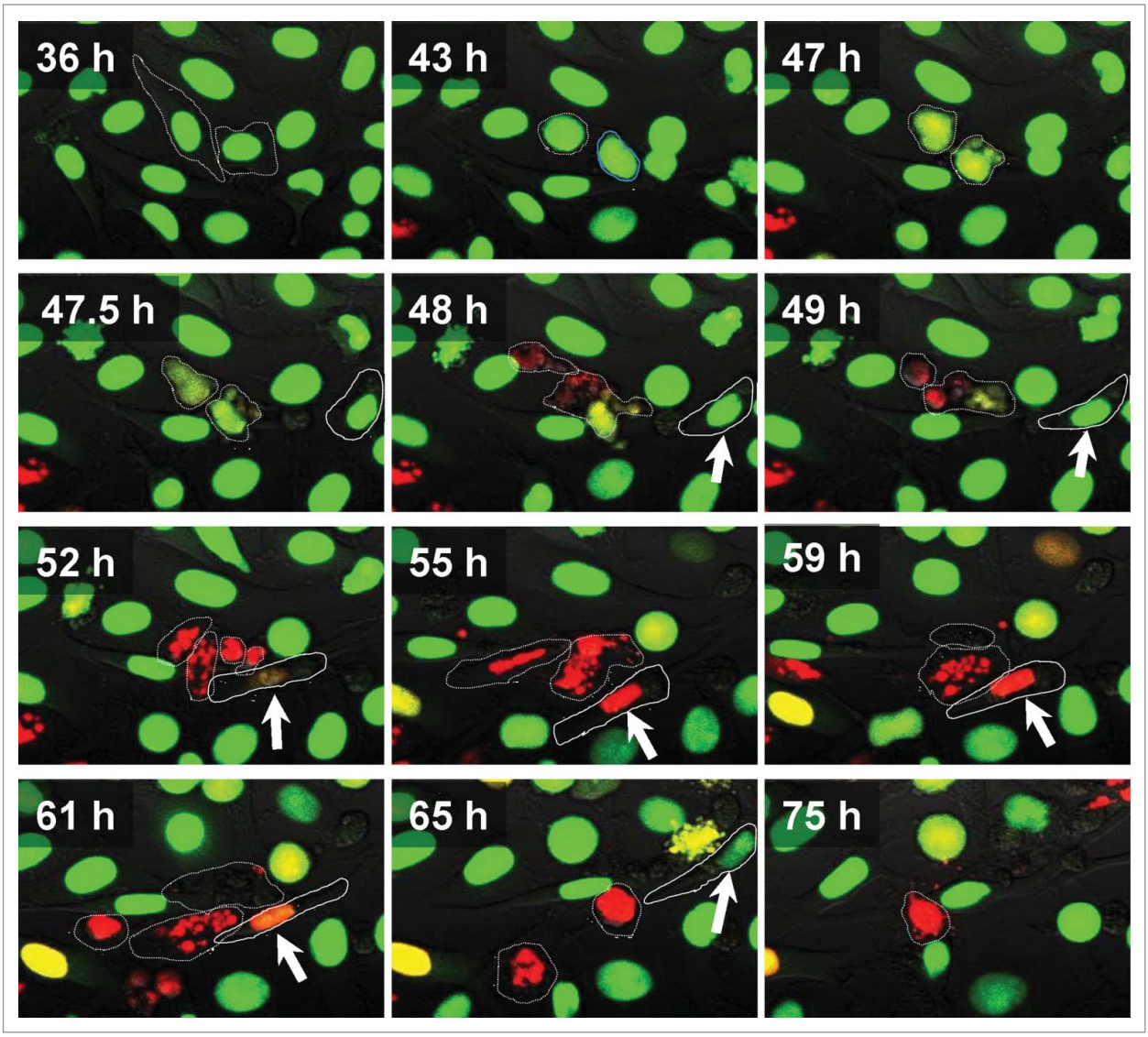

Figure 3. FUCCI imaging of cell-cycle progression and apoptosis after doxorubicin (DOX) treatment. The cells outlined with white dotted lines became apoptotic after mitosis. Arrows and cells outlined with white solid line(s) appeared to change from S/G_2/M phase to G_1 phase without mitosis. Time-lapse imaging of cells from 36h to 75h. At hour 48, note the start of mitosis. Between the hours of 52 and 55, note the onset of nuclear fragmentation.

phase. The fluorescent color of the cells changed from red to yellow, followed by green, indicating that the cells in G_1-phase entered early S-phase, followed by S/G_2/M phase. Nuclear fragmentations during cell cycle progression was rarely observed in these untreated cells (**Fig. 1**, **Video S1**).

Time-lapse FUCCI imaging of cell-cycle progression or arrest after treatment with doxorubicin

Time-lapse imaging of HeLa-FUCCI cells demonstrated that doxorubicin (DOX) induced their arrest in S/G_2/M phase within 24 h (**Fig. 2**). A subpopulation of the cells treated with DOX escaped cell cycle arrest and became apoptotic after mitosis (**Table 1**; **Figure 2B, C**; **Figure 3**; **Videos S2, S3, S4**). A small fraction of the cells appeared to change from green fluorescence to red without entering mitosis, indicating a possible reversal during the cell cycle. Mitosis correlated with reduced survival of the DOX-treated HeLa-FUCCI cells ($P < 0.001$) (**Fig. 4**). There was no significant correlation between

Table 2. Multivariate analysis of association between cell-cycle dynamics and apoptosis after DOX treatment

	HR	95% CI	*P*-value
G_1/S transition	0.477	0.270–0.846	0.011
Mitosis	4.945	3.128–7.817	< 0.001
Cell cycle phase at initiation of treatment	1.704	0.940–3.091	0.079

Abbrevations: CI, confidence interval; HR, hazard ratio.

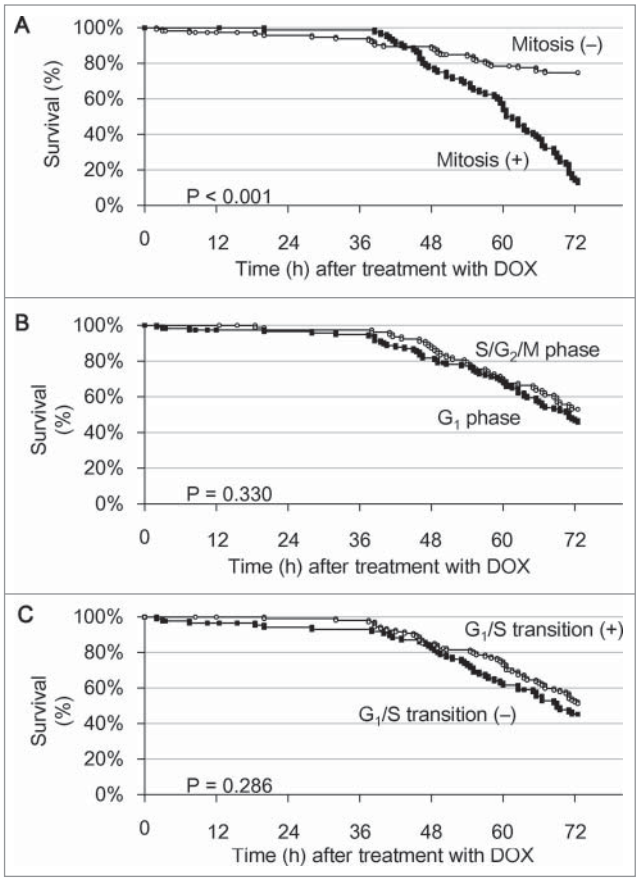

Figure 4. Survival analyses of individual cells treated with DOX. (**A**) Kaplan-Meier survival curve for the cells with or without mitosis. (**B**) Kaplan-Meier survival curve for the cells in each cell cycle phase at the beginning of drug treatment. **C.** Kaplan-Meier survival curve for the cells with or without transition from mitosis to G_1 to S phase.

Table 3. Cell-cycle fate analysis of HeLa-FUCCI cells after cisplatinum (CDDP) treatment

Parameters	Cell No.
Cell-cycle phase at the beginning of time-lapse imaging	
G_0/G_1 phase	107 (55.7%)
$S/G_2/M$ phase	85 (44.3%)
G_1/S transition during time-lapse imaging	
yes	136 (70.8%)
no	56 (29.2%)
Mitosis during time-lapse imaging	
yes	69 (35.9%)
no	123 (64.1%)
Cell-cycle "reversal" during time-lapse imaging[a]	
Yes	6 (3.1%)
No	186 (96.9%)
Apoptosis during time-lapse imaging	
yes	61 (31.8%)
no	131 (68.2%)

[a]Cells changing fluorescence color from FUCCI green to red without entering mitosis.

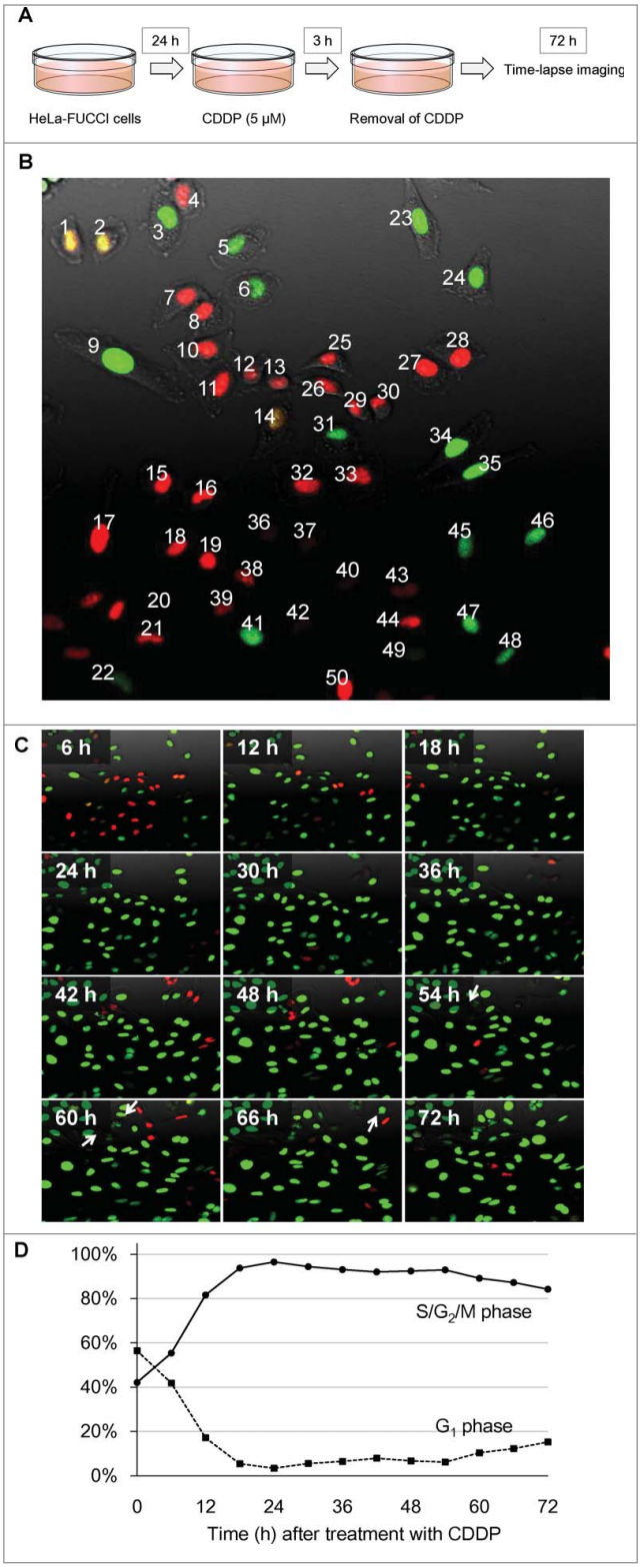

Figure 5. Single cell time-lapse FUCCI imaging in HeLa cells after treatment with cisplatinum (CDDP). (**A**) Study protocol. (**B**) Each cell was individualized by numbering, and the cell-cycle phase of each cell was observed for 72 hours. (**C**) Cell-cycle modulation and induction of apoptosis with CDDP. Arrows indicate apoptotic cells. (**C**) Distribution of cell-cycle phase after CDDP treatment.

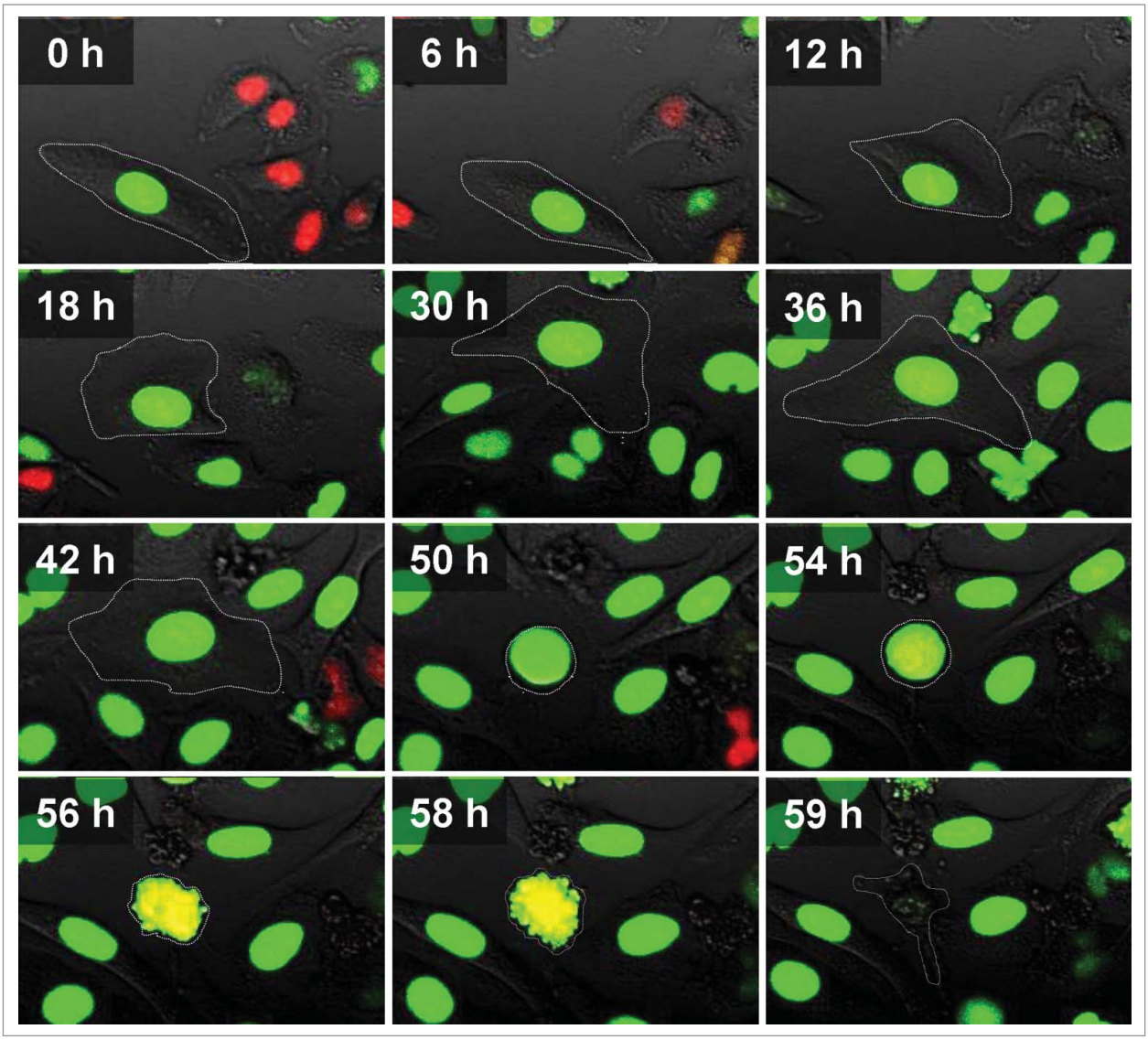

Figure 6. Mitosis and apoptosis after CDDP treatment. Some FUCCI-expressing HeLa cell imaged over 59 hours, become apoptotic before the completion of mitosis. Cells circled with white dotted lines became apoptotic after mitosis. At hour 56, note the appearance of yellow fluorescence due to co-expression of FUCCI green and red fluorescent proteins. At hour 58, note appearance of nuclear fragmentation due to apoptosis.

the cell-cycle phase in which DOX treatment started and cell survival (P = 0.330). There was also no significant correlation between the G_1/S transition and cell survival (P = 0.286) using the Kaplan-Meier test with log rank. However, multivariate analysis revealed that the G_1/S transition [hazard ratio (HR) = 0.477; P = 0.011] as well as mitosis (HR = 4.945; $P < 0.001$) significantly correlated positively and negatively, respectively, with cell survival (**Table 2**).

Time-lapse FUCCI imaging of cell cycle progression or arrest after treatment with cisplatinum

Time-lapse imaging of HeLa-FUCCI cells after treatment with cisplatinum (CDDP) (5 μm) demonstrated that more than 90% of the cells were arrested in S/G_2/M phases within 24 h after initation of treatment (**Table 3**; **Figure 5A-D**; Supp. Video 5, 6, 7). The cell-cycle arrest in S/G_2/M phases was maintained in more than 80% of the cells. However, time-lapse imaging demonstrated that a subpopulation of cells underwent mitosis. The daughter cells became red fluorescent and subsequently apoptotic (**Fig. 6**). Mitosis significantly decreased the survival of the cells ($P < 0.001$, **Fig. 7A**). Treatment initiation of cells with CDDP during S/G_2/M phases also significantly decreased cell survival (P = 0.003, **Fig. 7B**). The transition from G_1 to S phase was significantly associated with increased cell survival ($P < 0.001$, as determined by Kaplan-Meier and log rank) (**Fig. 7C**).

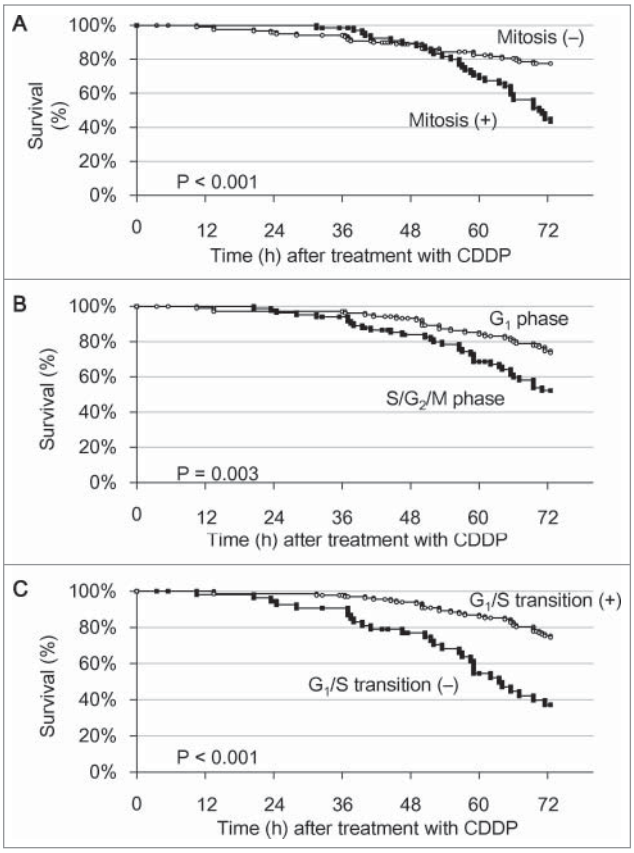

Figure 7. Survival analyses of individual cells treated with CDDP. (**A**) Kaplan-Meier survival curve for the cells with or without mitosis. (**B**) Kaplan-Meier survival curve for the cells in each cell cycle phase at the beginning of treatment. (**C**) Kaplan-Meier survival curve for the cells with or without transition from mitosis to G_1 to S phase.

Multivariate analysis also demonstrated that the transition from G_1 to S phase (HR = 0.241; $P < 0.001$) as well as mitosis (HR = 2.936; $P < 0.001$) were independent factors influencing cell survival (**Table 4**).

Before DOX or CDDP treatment, approximately 60% of the HeLa-FUCCI cells were in G_1/G_0 phase and 40% of the cells were in $S/G_2/M$ phase. A large subpopulation of the treated cells arrested in $S/G_2/M$ phase. There was a difference in the apoptotic responses to DOX and CDDP. DOX induced apoptosis immediately after mitosis, whereas CDDP induced apoptosis before, as well as after, completion of mitosis.

Previously, studies of the cell cycle used flow cytometry, western blotting, or other non-real-time methods.[29] Sakaue-Sawano et al.[22] developed FUCCI, enabling real-time single-cell analysis

Table 4. Multivariate analysis for association between cell cycle dynamics and apoptosis after CDDP treatment

	HR	95% CI	*P*-value
G_1/S transition	0.241	0.132–0.438	< 0.001
Mitosis	2.936	1.720- 5.011	< 0.001
Cell cycle phase at initiation of treatment	1.499	0.806- 2.790	0.201

Abbrevations: CI, confidence interval; HR, hazard ratio.

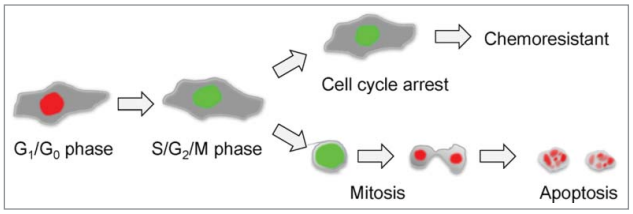

Figure 8. Schema of correlation between chemosensitivity and cell-cycle phase after drug treatment. DOX and CDDP induced cell-cycle arrest in $S/G_2/M$ phase. Survival analyses indicated that cells which escaped cell-cycle arrest and entered mitosis subsequently became apoptotic.

of the cell cycle. In the present study, single-cell time-lapse FUCCI imaging enabled observation of the cell-cycle progression in each cell and subsequent apoptotic changes after treatment with chemotherapy drugs.

Mitosis, cell-cycle blockage in $S/G_2/M$ and the G_1/S transition after treatment with anticancer drugs significantly correlated with survival of the cells (**Fig. 8**). Our study is also the first report which determined independent predictive factors for chemosensitivity or chemoresistance using univariate and multivariate analyses of individual cells.

The present results demonstrated that chemoresistant cells can be readily identified in a heterogeneous population of cancer cells and can serve in future studies as visual targets for novel agents that kill arrested and thereby chemoresistant cancer cells.

Previously-developed concepts and strategies of highly-selective tumor-targeting[30-37] can take advantage of monitoring the cell-cycle fate of treated FUCCI-expressing cancer cells described in the present report.

In summary, FUCCI time-lapse imaging enabled dynamic observation of cell cycle progression in each cancer cell. Both DOX and CDDP induced cell-cycle arrest in $S/G_2/M$ phases in the majority of the cells. Some cells however entered mitosis. The cells treated with DOX became apoptotic after mitosis, whereas cells treated with CDDP became apoptotic before, as well as after. Multivariate survival analyses of single-cell FUCCI imaging data indicated that G_1/S transition significantly correlated with increased cell survival and mitosis significantly decreased the survival of the cells after treatment with DOX or CDDP. Treatment with both drugs indicated heterogeneity of response in the cancer cell population.

Materials and Methods

Establishment of HeLa cells stably transfected with FUCCI vector plasmids

mKO2-hCdt1 (green fluorescent protein) and mAG-hGem (orange fluorescent protein)[22] were obtained from the Medical & Biological Laboratory (Nagoya, Japan). mKO2-hCdt1 and mAG-hGem were transfected into HeLa cells using Lipofectamine™ LTX (Invitrogen, Carlsbad, CA). HeLa cells were incubated for 48 h after transfection with mK02-hCdt1, and were then trypsinized and seeded in 96-well plates. Cells were then sorted by green fluorescence (S, G_2, and M phase) cells using a

FACSAria cell sorter (Becton Dickinson). The first-step-sorted green-fluorescent cells were then transfected with mAG-hGem (orange) and then sorted by orange fluorescence.

Time-lapse FUCI imaging of the cell-cycle and response to anticancer drugs

HeLa-FUCCI cells were cultured in high-glucose DMEM (Invitrogen, Carlsbad, CA) with 10% fetal bovine (FBS) (Sigma-Aldrich, St. Louis, MO) at 37°C with 95% air and 5% CO_2 for 24 h. The cells were treated with DOX (5 μM) or CDDP (5 μM) for 3 h. After treatment, cell-cycle progression and apoptosis were observed every 30 min for 72 h using a FluoView FV1000 confocal laser microscope (Olympus Corp., Tokyo, Japan).[38] Scanning and image acquisition were controlled by FluoView software (Olympus).

Statistical analysis

The cell survival period of each cell was defined as the time from the initial imaging after treatment to the time of death or appearance of apoptosis. Survival was calculated using the Kaplan–Meier method along with the log rank test. In addition, the Cox proportional hazards regression model was used for multivariate analyses to identify independent factors which correlate with survival of the cancer cells. Statistical significance was defined as $P \leq 0.05$. Statistical analyses were performed using the EZR statistical software (Saitama Medical Center, Jichi Medical University, Saitama, Japan).

Disclosure of Potential Conflicts of Interest

S.M., S.Y., H.K., M.Y., M.T., Y.M., F.U., Y.H., T.M., K.H., N.Y. and R.M.H. are or were unsalaried associates of AntiCancer Inc. There are no other competing financial interests.

Dedication

This paper is dedicated to the memory of A.R. Moossa, MD.

Funding

This work was supported by NIH grant CA132971 and Grant-in-Aid for Young Japanese Scientists (B) 50608693.

Supplemental Material

Supplemental data for this article can be accessed on the publisher's website.

References

1. Levan A, Hauschka TS. Endomitotic reduplication mechanisms in ascites tumors of the mouse. J Natl Cancer Inst 1953; 14:1-21; PMID:13097135
2. Klein G, Klein E. Conversion of solid neoplasms into ascites tumors. Ann NY Acad Sci 1956; 63:640-61; PMID:13314425; http://dx.doi.org/10.1111/j.1749-6632.1956.tb50883.x
3. Makino S. Further evidence favoring the concept of the stem cell in ascites tumors of rats. Ann NY Acad Sci 1956; 63:818-30; PMID:13314436; http://dx.doi.org/10.1111/j.1749-6632.1956.tb50894.x
4. Henderson JS, Rous P. The plating of tumor components on the subcutaneous expanses of young mice. J Exp Med 1962; 115:1211-30; PMID:NOT_FOUND; http://dx.doi.org/10.1084/jem.115.6.1211
5. Gray JM, Pierce GB. Relationship between growth rate and differentiation of melanoma in vivo. J Natl Cancer Inst 1964; 32:1201-11; PMID:14191394
6. Prehn RT. Analysis of antigenic heterogeneity within individual 3-methylcholanthrene-induced mouse sarcomas. J Natl Cancer Inst 1970; 45:1039-45; PMID:18605432
7. Mitelman F. The chromosomes of fifty primary Rous rat sarcomas. Hereditas 1971; 69:155-86; PMID:4376138; http://dx.doi.org/10.1111/j.1601-5223.1971.tb02431.x
8. Foulds L. Neoplastic Development, Vol. 1. New York: Academic Press, Inc., 1969.
9. Foulds L. Neoplastic Development, Vol. 2. New York: Academic Press, Inc., 1975.
10. Fidler IJ, Kripke ML. Metastasis results from preexisting variant cells within a malignant tumor. Science 1977; 197:893-5; PMID:887927; http://dx.doi.org/10.1126/science.887927
11. Cifone MA, Fidler IJ. Increasing metastatic potential is associated with increasing genetic instability of clones isolated from murine neoplasms. Proc Natl Acad Sci USA 1981; 78: 6249-52.
12. De Baetseher P, Gorelik E, Eshhar Z, Ron Y, Katzav S, Feldman M, Segal S. Metastatic properties conferred on nonmetastatic tumors by hybridization of spleen B-lymphocytes with plasmacytoma cells. J Natl Cancer Inst 1981; 67:1079-87; PMID:6975387
13. Kerbel RS, Dennis JW, Largante AE, Frost P. Tumor progression in metastasis: an experimental approach using lectin resistant tumor variants. Cancer Metastasis Rev 1982; 1:99-140; http://dx.doi.org/10.1007/BF00048223
14. Heppner GH. Tumor heterogeneity. Cancer Res 1984; 44:2259-65; PMID:6372991
15. Heppner GH, Miller BE. Therapeutic implications of tumor heterogeneity. Semin Oncol 1989; 16:91-105; PMID:2652316
16. Goldie JH, Goldman AJ. A mathematical model for relating the drug sensitivity of tumors to their spontaneous mutation rate. Cancer Treat Rep 1979; 63:1727-33; PMID:526911
17. Schöber C, Gibbs JF, Yin MB, Slocum HK, Rustum YM. Cellular heterogeneity in DNA damage and growth inhibition induced by ICI D1694, thymidylate synthase inhibitor, using single cell assays. Biochem Pharmacol 1994; 48:997-1002; PMID:8093112; http://dx.doi.org/10.1016/0006-2952(94)90370-0
18. Slocum HK, Parsons JC, Winslow EO, Broderick L, Minderman H, Tóth K, Greco WR, Rustum YM. Time-lapse video reveals immediate heterogeneity and heritable damage among human ileocecal carcinoma HCT-8 cells treated with raltitrexed (ZD1694). Cytometry 2000; 41:252-60; PMID:11084610; http://dx.doi.org/10.1002/1097-0320(20001201)41:4%3c252::AID-CYTO3%3e3.0.CO;2-X
19. Yin MB, Voigt W, Panadero A, Vanhoefer U, Frank C, Pajovic S, Azizkhan J, Rustum YM. p53 and WAF1 are induced and Rb protein is hypophosphorylated during cell growth inhibition by the thymidylate synthase inhibitor ZD1694 (Tomudex). Mol Pharmacol 1997; 51:630-6; PMID:9106628
20. Matsui SI, Arredondo MA, Wrzosek C, Rustum YM. DNA damage and p53 induction do not cause ZD1694-induced cell cycle arrest in human colon carcinoma cells. Cancer Res 1996; 56:4715-23.
21. Bhatia S, Frangioni JV, Hoffman RM, Iafrate AJ, Polyak K. The challenges posed by cancer heterogeneity. Nature Biotech 2012; 30:604-10; http://dx.doi.org/10.1038/nbt.2294
22. Sakaue-Sawano A, Kurokawa H, Morimura T, Hanyu A, Hama H, Osawa H, Kashiwagi S, Fukami K, Miyata T, Miyoshi H, et al. Visualizing spatiotemporal dynamics of multicellular cell-cycle progression. Cell 2008; 132:487-98; PMID:18267078; http://dx.doi.org/10.1016/j.cell.2007.12.033
23. Yano S, Miwa S, Mii S, Hiroshima Y, Uehara F, Yamamoto M, Kishimoto H, Tazawa H, Bouvet M, Fujiwara T, et al. Invading cancer cells are predominantly in G0/G1 resulting in chemoresistance demonstrated by real-time FUCCI imaging. Cell Cycle 2014; 13:953-60; PMID:24552821; http://dx.doi.org/10.4161/cc.27818
24. Miwa S, Yano S, Tome Y, Sugimoto N, Hiroshima Y, Uehara F, Mii S, Kimura H, Hayashi K, Efimova EV, et al. Dynamic color-coded fluorescence imaging of the phase mitosis, and apoptosis demonstrates how caffeine modulates cisplatinum efficacy. J Cell Biochem 2013; 114:2454-60; PMID:23696238; http://dx.doi.org/10.1002/jcb.24593
25. Yano S, Zhang Y, Zhao M, Hiroshima Y, Miwa S, Uehara F, Kishimoto H, Tazawa H, Bouvet M, Fujiwara T, et al. Tumor-targeting Salmonella typhimurium A1-R decoys quiescent cancer cells to cycle as visualized by FUCCI imaging and become sensitive to chemotherapy. Cell Cycle 2014, 13:3958-63.
26. Blagosklonny MV. Mitotic arrest and cell fate: why and how mitotic inhibition of transcription drives mutually exclusive events. Cell Cycle 2007; 6:70-4; PMID:17245109; http://dx.doi.org/10.4161/cc.6.1.3682
27. Blagosklonny MV. The power of chemotherapeutic engineering: arresting cell cycle and suppressing senescence to protect from mitotic inhibitors. Cell Cycle 2011; 10:2295-8; PMID:21715978; http://dx.doi.org/10.4161/cc.10.14.16819
28. Leontieva OV, Gudkov AV, Blagosklonny MV. Weak p53 permits senescence during cell cycle arrest. Cell Cycle 2010; 9:4323-7; PMID:21051933; http://dx.doi.org/10.4161/cc.9.21.13584
29. Mueller S, Schittenhelm M, Honecker F, Malenke E, Lauber K, Wesselborg S, Hartmann JT, Bokemeyer C, Mayer F. Cell-cycle progression and response of germ cell tumors to cisplatinum in vitro. Int J Oncol 2006; 29:471-9; PMID:16820891

30. Blagosklonny MV. How cancer could be cured by 2015. Cell Cycle 2005; 4:269-78; PMID:15655345
31. Blagosklonny MV. Tissue-selective therapy of cancer. Br J Cancer 2003; 89:1147-51; PMID:14520435; http://dx.doi.org/10.1038/sj.bjc.6601256
32. Blagosklonny MV. Matching targets for selective cancer therapy. Drug Discov Today 2003; 8:1104-7; PMID:14678733; http://dx.doi.org/10.1016/S1359-6446(03)02806-X
33. Blagosklonny MV. "Targeting the absence" and therapeutic engineering for cancer therapy. Cell Cycle 2008; 7:1307-12; PMID:18487952; http://dx.doi.org/10.4161/cc.7.10.6250
34. Blagosklonny MV. Teratogens as anti-cancer drugs. Cell Cycle 2005; 4:1518-21; PMID:16258270; http://dx.doi.org/10.4161/cc.4.11.2208
35. Blagosklonny MV. Treatment with inhibitors of caspases, that are substrates of drug transporters, selectively permits chemotherapy-induced apoptosis in multidrug-resistant cells but protects normal cells. Leukemia 2001; 15:936-41; PMID:11417480; http://dx.doi.org/10.1038/sj.leu.2402127
36. Blagosklonny MV. Target for cancer therapy: proliferating cells or stem cells. Leukemia 2006; 20:385-91; PMID:16357832; http://dx.doi.org/10.1038/sj.leu.2404075
37. Blagosklonny MV. Cancer stem cell and cancer stemloids: from biology to therapy. Cancer Biol Ther 2007; 6:1684-90; PMID:18344680; http://dx.doi.org/10.4161/cbt.6.11.5167
38. Uchugonova A, Zhao M, Weinigel M, Zhang Y, Bouvet M, Hoffman RM, Koenig K. Multiphoton tomography visualizes collagen fibers in the tumor microenvironment that maintain cancer-cell anchorage and shape. J Cell Biochem 2013; 114:99-102.